

Investigation of the Effects of Optical Models on the Production Cross-Section Calculations of $^{22,24}\text{Na}$ Radioisotopes with some (d,x) and (α ,x) Reactions

Mert Şekerci ^{1*}

¹Süleyman Demirel University, Department of Physics, 32260, Isparta, TÜRKİYE

Received:27/09/2022, **Revised:** 13/12/2022, **Accepted:** 27/12/2022, **Published:** 30/12/2022

Abstract

The results of the research carried out in the field of basic sciences and the achievements obtained in these studies mediate effective and beneficial results not only for basic sciences, but also in many various fields from medicine to engineering. In this context, the theoretical investigation of the production routes of various radioisotopes, that can be used in many fields, ensures that physics and other related fields meet on a common denominator. Considering this fact as motivation, the aim of this study is to investigate how various deuteron and alpha optical models affect the cross-section calculations of $^{22,24}\text{Na}$ radioisotopes, which are known to be used in medical applications. The TALYS (v1.95) code was utilized in the calculations, which allows for the use of five different deuteron and eight different alpha optical model alternatives. The obtained results were not only visually compared to the existing experimental data in the literature, but also quantitatively by performing mean weighted deviation and relative variance analyses.

Keywords: cross-section, radioisotope, theoretical model, TALYS

Bazı (d,x) ve (α ,x) Reaksiyonlarıyla $^{22,24}\text{Na}$ Radyoizotoplarının Üretim Tesir Kesiti Hesaplamalarına Optik Modellerin Etkilerinin İncelenmesi

Öz

Temel bilimler alanında yürütülen araştırmaların sonuçları ve bu çalışmalarda elde edilen kazanımlar sadece temel bilimler için değil, aynı zamanda tıptan mühendisliğe kadar pek çok çeşitli alanda da etkili ve faydalı sonuçlara aracılık etmektedir. Bu bağlamda, birçok alanda kullanılabilecek çeşitli radyoizotopların üretim yollarının teorik olarak araştırılması, fizik ve diğer ilgili alanların ortak bir paydada buluşmasını sağlamaktadır. Motivasyon olarak bu gerçek göz önünde bulundurularak bu çalışmanın amacı, çeşitli döteron ve alfa optik modellerin tıbbi uygulamalarda kullanıldığı bilinen $^{22,24}\text{Na}$ radyoizotoplarının tesir kesiti hesaplamalarını nasıl etkilediğini araştırmak olarak belirlenmiştir. Hesaplamalarda beş farklı döteron ve sekiz farklı alfa optik model alternatifinin kullanımına olanak sağlayan TALYS (v1.95) kodu kullanılmıştır. Elde edilen sonuçlar literatürdeki mevcut deneysel verilerle sadece görsel olarak değil, ortalama ağırlıklı sapma ve bağıl varyans analizleri yapılarak nicel olarak da karşılaştırılmıştır.

Anahtar Kelimeler: tesir kesiti, radyoizotop, teorik model, TALYS

*Corresponding Author: mertsekerci@sdu.edu.tr

Mert Şekerci, <https://orcid.org/0000-0003-0870-0506>

1. Introduction

Not only the results of scientific research, but also the various gains obtained during the realization of these researches provide valuable inferences that can guide both the literature and subsequent studies. Indeed, theoretical studies, particularly in natural sciences, are as significant and valuable as experimental ones. Furthermore, this circumstance motivates the development of interdisciplinary research studies oriented on common bases, which can influence and benefit one another by using the obtained results [1-3]. Theoretical studies are undoubtedly significant in physics, as they are in many other disciplines, particularly in related fields of research that might be included into nuclear physics. Many factors, which may differ depending on the investigated topic, such as technological and physical infrastructure, financial capacity, and trained manpower, are critical to the effective completion of experimental research. In the event that an experimental study, which have to be designed by combining these and many other possible factors in a functional way, cannot be realized, the way for researchers to have a foresight on the subject they are examining can be obtained from theoretical studies and computer-aided simulations [4-13]. An essential consideration here is that the involvement of a theoretical basis is required in both circumstances, whether an experimental research or computer-aided modeling study. In this context, it is evident from the studies in the previously shown literature that many models have been developed to comprehensively examine and analyze nuclear reaction mechanisms and processes. There are multiple values that can be examined in nuclear reaction processes, which are known to exist in a wide range from the formation of the universe to the applications that affect our daily lives. The cross-section quantity, which may be defined as the likelihood of a nuclear reaction take place, is one of the most remarkable among them. This value can be measured by experimental studies as well as calculated theoretically, and its presence is very important in interpreting the process and details of a nuclear reaction [14-16]. It is a known fact that nuclear models and the varied parameters of these models affect the calculation outcomes of the cross-section values, and there are also models called optical models among these models. As a consequence, investigations on the influences of optical models on the cross-section calculations will undoubtedly contribute to the literature. The cross-section calculations include complicated mathematical procedures and operations that make use of theoretical models and parameters. When the hand-made aspect comes into effect, repeating these steps several times for varying values of a parameter creates a very high chance of inaccuracy and mistake. As a response, several computer-aided calculation tools have been developed to address situations where the cross-section values are theoretically tried to be acquired. Some of these can be shown as ALICE/ASH [17], CEM95 [18, 19], PCROSS [20], and most commonly employed codes EMPIRE [21] and TALYS [22, 23].

In this study, the 1.95 version of the TALYS code, which has a high utilization rate in the literature, was chosen. The goal of this study using the TALYS code is to look at the impact of five distinct deuteron and eight different alpha optical model potentials on the production cross-section calculations of $^{22,24}\text{Na}$ radioisotopes that are known to be employed in medical applications. Even a brief review of the literature will reveal numerous clinical studies on the use of several radioisotopes in medical applications. Similarly, various theoretical

investigations on these radioisotopes can be seen in the literature. In these studies, it is generally aimed to investigate the effects of including different models and parameters in the calculations, and it is seen that they contribute to both the development of theoretical models and the research of existing and new production routes of significant radioisotopes [24-27]. The reactions investigated in this study for the production of $^{22,24}\text{Na}$ radioisotopes are some (d,x) and (α ,x) reactions on $^{\text{nat}}\text{Mg}$ which are; $^{\text{nat}}\text{Mg}(\text{d},\text{x})^{22}\text{Na}$, $^{\text{nat}}\text{Mg}(\text{d},\text{x})^{24}\text{Na}$, $^{\text{nat}}\text{Mg}(\alpha,\text{x})^{22}\text{Na}$ and $^{\text{nat}}\text{Mg}(\alpha,\text{x})^{24}\text{Na}$. For these reactions, graphical representations were presented in which the theoretical data obtained from the results of the calculations performed by using different models and the experimental data obtained from the literature are given jointly so the outcomes could be analyzed visually. In addition to the graphical representations, the mean weighted deviation [28] and relative variance analyses [28] were performed in order to analyze the outcomes quantitatively.

2. Material and Methods

The radioisotopes $^{22,24}\text{Na}$ included in this study are among the several radioisotopes that are widely used in medicinal applications. Sodium has twenty known isotopes, of which only ^{23}Na is stable, and two isomers. Half-lives of isotopes other than ^{22}Na and ^{24}Na have been reported to be less than one minute, and often less than one second [29, 30]. Sodium, an alkali metal, is the seventh most prevalent element in the earth's crust, accounting for around 2.27 % of the total, and is critical for life [31]. The half-life of ^{22}Na (decay modes: ec (electron capture) β^+ (emission of an anti-electron and a neutrino) 100 %, Q_{β^-} (energy available for β^- decay): -4781.41 ± 0.16 keV, Q_{α} (energy available for α decay): -8479.4 ± 0.5 keV, Q_{EC} (energy available for EC decay): 2843.33 ± 0.13 keV) is 2.6019 years, while the half-life of ^{24}Na (decay modes: β^- (emission of an electron and an anti-neutrino) 100 %, Q_{β^-} (energy available for β^- decay): 5515.677 ± 0.021 keV, Q_{α} (energy available for α decay): -10825.35 ± 0.03 keV, Q_{EC} (energy available for EC decay): -2466.3 ± 0.5 keV) is 14.9560 hours [32]. Given the characteristic properties of ^{22}Na , its usage for a number of applications and differ purposes, such as calibration in positron emission tomography (PET) imaging systems, has emerged [33-36]. On the other side, ^{24}Na has been demonstrated to be useful in studies on bone blood flow, postmastectomy lymphedema, intramuscular clinical trials, and noradrenaline sensitivity in hypertension [37-41]. Apart from these studies, it is possible to encounter examples of studies on the use of both radioisotopes for different purposes in the literature [42-45].

In this study, $^{22,24}\text{Na}$ isotopes were prioritized since their values could be easily realized when current and potential usage areas and the benefits they provide are considered together. In this context, production cross-section calculations were made for $^{22,24}\text{Na}$ radioisotopes in reactions with deuteron and alpha incident particles onto $^{\text{nat}}\text{Mg}$. The factor that constitutes the remarkable point of this study is directly related to how these calculations are made. In this process, different optical model potentials were imposed on the calculations and how the outcomes differ as a result of this situation was examined. As mentioned in the previous section, it is a known situation that there are many programs and tools that can be used to calculate the cross-section value. It can be easily seen from the literature that TALYS code is preferred more frequently than others among these mentioned tools. Some of the examples for this situation could be given

as follows; free and open source code distribution, there is no special training required to use the code at the beginner level, the ability to automatically or optionally adjust various parameters according to the user's level of knowledge and code mastery, diversity and choice to allow the investigations of various nuclear reaction models and the effects of many parameters on different calculations, etc. In this study, TALYS code was preferred due to its competencies and the availability of multiple optical model potentials offered to the users in order to examine the effects of deuteron and alpha optical model potentials on the calculation results.

Before describing the deuteron and alpha optical model potentials that can be utilized in the TALYS code, it will be appropriate to address the optical model expression first. This expression denotes an inherently complex interaction between a particle arriving at a nucleus with a complex mean field potential. The complex mean field potential present in the interaction causes the flux of the reaction formed to split into two parts, one for generating elastic scatterings and the other for all other channels. In the TALYS code, a subprogram called ECIS-06 [46] is used for these complex optical model calculations, and all optical model calculations are first performed for all potential outgoing particle paths and energies and recorded. In the next step, the corresponding conduction coefficients can be used in the calculations for pre-equilibrium and compound nucleus. Finally, calculations are made for each incoming energy value given by the user. The study that Koning and Rochman brought to the literature can be examined for more detailed information on this subject [47].

The models and parameters available to the users in the TALYS code version 1.95, which is the utilized version in this study, are actually used by replacing the pre-defined, or other words default-assigned, models and parameters with specific keywords. There are five different options in the TALYS code for the deuteron optical model potential examined in this study. The Normal deuteron potential is the TALYS code's standard deuteron optical model, which is generated by simplifying Watanabe's folding technique [48]. Apart from this, users can choose the deuteron optical models that have been brought to the literature as a result of the studies of Daehnick et al. [49], Bojowald et al. [50], Han et al. [51] and An and Cai's [52]. In this study, the impacts of all of these models on computations are investigated, and they will be denoted as DOMP1, DOMP2, DOMP3, DOMP4, and DOMP5 in the rest of the article, in the sequence provided above.

After mentioning the deuteron optical models, now it is the place to move on to the alpha optical models that are available in the TALYS code. The TALYS code allows users to select from eight alternative alpha optical model potentials. One of these possibilities has been adopted as the default model by TALYS for the alpha optical model potential, the one imposed by Avrigeanu et al.'s [53] study. Other than the default option, one other option is named as Normal Alpha Potential and is listed as the first option in the TALYS code [48, 54]. Even though it may appear to be a bit outdated, another model that can still be favored in certain situations, depending on the content and character of research, is presented as the second alternative, and this model is taken from McFadden and Satchler's study [55]. The TALYS code presents three possible choices for Demetriou et al.'s [56] double folding potential. The distinction among these three options is that the first two alternatives employ tables, but the third uses the

dispersion model. Another possibility is based on Nolte et al.'s work [57], which developed a set of parameters for the global optical potential of alpha particles with energy of more than 80 MeV. In another study carried out by Avrigeanu et al. [58], the definition of spherical optical potential defined for alpha particles with energies above 80 MeV was extended to lower energies. The remaining alpha optical model potential in the TALYS code, which has not been mentioned so far, is developed on the basis of this study. The abbreviations of the alpha optical models used in this study are shown with the prefix AOMP and the model names are given between AOMP1-AOMP8 since there are eight options in total.

The evaluation of the calculation results obtained for the reactions examined within the scope of the study and the analysis of their compatibility with the experimental data was made both visually and numerically. Both the computation findings and the accessible experimental data from Experimental Nuclear Reaction Data (EXFOR) [59, 60] are shown together for visual interpretation. For numerical analysis, mean weighted deviation (F) and relative variance (D) calculations were made using the equations given in Equations 1 and 2, respectively [28].

$$F = \left[\frac{1}{n} \sum_{i=1}^n [(\sigma_i^{calc} - \sigma_i^{expr}) / \Delta\sigma_i^{expr}]^2 \right]^{1/2} \quad (1)$$

$$D = \left[\frac{1}{n} \sum_{i=1}^n |\sigma_i^{calc} - \sigma_i^{expr}| / \sigma_i^{expr} \right] \quad (2)$$

As can be seen, both equations have σ_i^{calc} and σ_i^{expr} expressions. Of these, σ_i^{calc} represents the calculated values, while σ_i^{expr} is the experimental data. Apart from these, N is used to represent the number of experimental data, and $\Delta\sigma_i^{expr}$ expression is used to represent the amount of error in each experimental data. It may be questionable by some readers why two values, both F and D , are used for numerical analysis, but there is a very logical explanation for this. Of these values, D only compares the calculation results with the experimental data, while F also considers the experimental error margins as a parameter in the calculations.

3. Results and Discussion

In this section, the outcomes of the calculations obtained as a result of separately triggering five different deuteron optical models, each of which is available in the TALYS code, for the $^{nat}\text{Mg}(d,x)^{22}\text{Na}$, $^{nat}\text{Mg}(d,x)^{24}\text{Na}$, $^{nat}\text{Mg}(\alpha,x)^{22}\text{Na}$ and $^{nat}\text{Mg}(\alpha,x)^{24}\text{Na}$ reactions examined within the scope of the study are interpreted. In this context, the visual analyses of the results obtained are presented in the illustrations given in Figures 1-4, while the results of the F and D values used in the numerical analyses are given in Tables 1 and 2.

Figure 1 shows the calculation results obtained for the $^{nat}\text{Mg}(d,x)^{22}\text{Na}$ reaction and the experimental data of Hermanne et al. [61] and Vlasov et al. [62] available in the literature. As can be seen from the figure, the calculation results obtained by using the models were able to relatively form a structure similar to the distribution formed by the experimental data. However, it should be taken into account that the experimental data of Vlasov et al. [62] up to about 15 MeV are higher than the other experimental data and calculations made with all models, especially in the peak region of the hump. In the figure where it is seen that the experimental data of Hermanne et al. [61] continue up to about 50 MeV, the calculation results obtained with

the models also show a similar distribution, but especially after 40 MeV, the results were obtained with higher values than the experimental data. Considering the whole energy range, it can be seen that DOMP2, DOMP 3, DOMP 4 and DOMP5 models produce results that are more discrete than DOMP1 and closer to each other. As a result, it can be easily interpreted from the visual that DOMP1 is the model that produces the most compatible results with the experimental data in the entire energy range, and from the F and D values in Table 1, where the numerical calculation results are presented.

Table 1. The values of the statistical parameters calculated for deuteron optical model potentials

Reaction	Parameters	DOMP1	DOMP2	DOMP3	DOMP4	DOMP5
$^{nat}\text{Mg}(d,x)^{22}\text{Na}$	F	10.3703	14.2388	16.4356	14.9810	14.9040
	D	0.7313	0.7856	0.8488	0.8234	0.8120
$^{nat}\text{Mg}(d,x)^{24}\text{Na}$	F	3.5882	4.9305	5.2074	4.7788	4.8806
	D	0.2959	0.4589	0.4967	0.4280	0.4570

Table 2. The values of the statistical parameters calculated for alpha optical model potentials

Reaction	Parameters	AOMP1	AOMP2	AOMP3	AOMP4	AOMP5	AOMP6	AOMP7	AOMP8
$^{nat}\text{Mg}(\alpha,x)^{22}\text{Na}$	F	3.6999	3.9956	5.8199	3.7642	3.8376	3.5740	3.7833	3.6498
	D	0.2080	0.2332	0.3746	0.2130	0.2006	0.2021	0.2083	0.2012
$^{nat}\text{Mg}(\alpha,x)^{24}\text{Na}$	F	6.6553	6.8679	6.9307	6.6411	6.6353	6.3836	6.5399	6.5086
	D	0.3679	0.4214	0.4137	0.3662	0.3743	0.3645	0.4075	0.3738

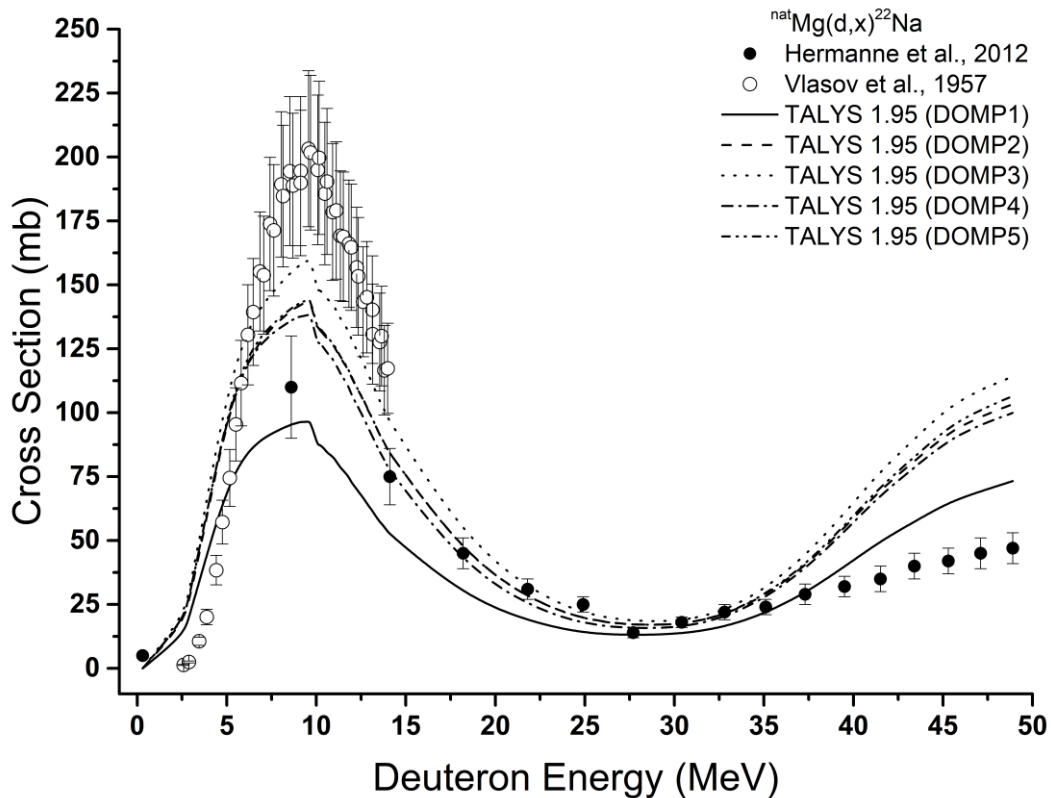


Figure 1. Calculation results and experimental data for the $^{nat}\text{Mg}(d,x)^{22}\text{Na}$ reaction

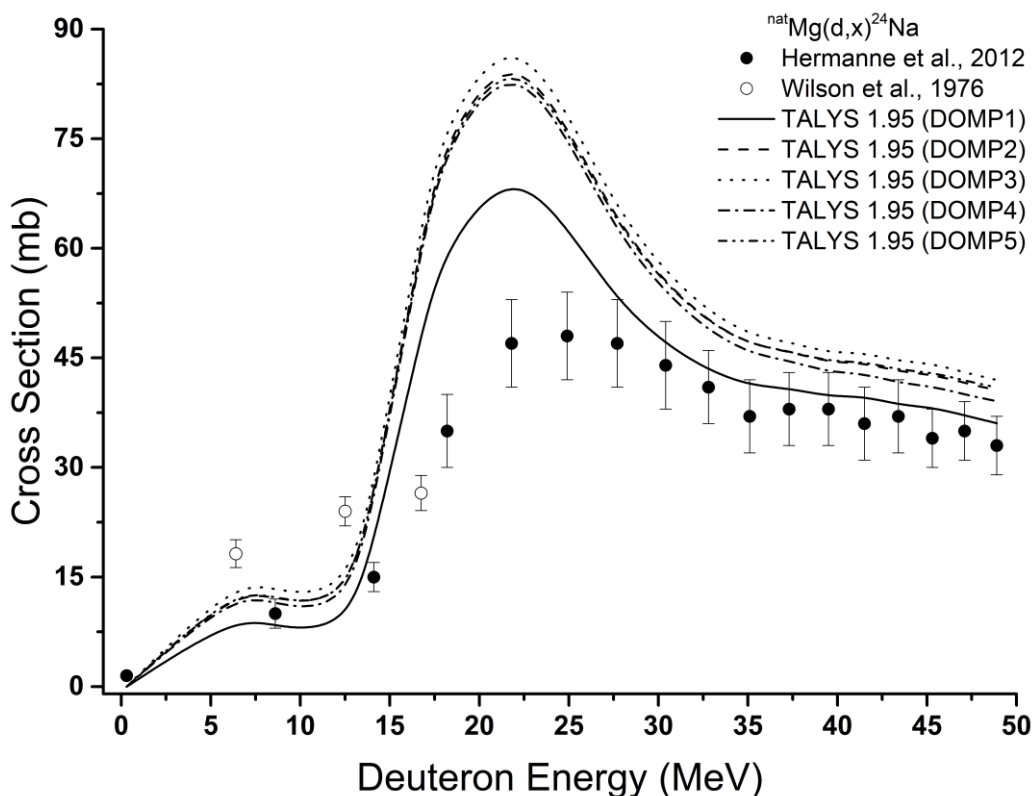


Figure 2. Calculation results and experimental data for the $^{\text{nat}}\text{Mg}(\text{d},\text{x})^{24}\text{Na}$ reaction

The calculation results of $^{\text{nat}}\text{Mg}(\text{d},\text{x})^{24}\text{Na}$, other deuteron input reaction investigated in this study, are depicted in Figure 2 together with the experimental data of Hermanne et al. [61] and Wilson et al. [63]. Although the incident particle energy shown on the x -axis is up to approximately 50 MeV in both $^{\text{nat}}\text{Mg}(\text{d},\text{x})^{22}\text{Na}$ and $^{\text{nat}}\text{Mg}(\text{d},\text{x})^{24}\text{Na}$ reactions, the difference between the order of the cross-section values shown on the y -axis is quite clear. On the other hand, similar to the $^{\text{nat}}\text{Mg}(\text{d},\text{x})^{22}\text{Na}$ reaction, the DOMP2, DOMP3, DOMP 4 and DOMP 5 models were very close to each other and produced different results from DOMP1 in this reaction, just as they did in $^{\text{nat}}\text{Mg}(\text{d},\text{x})^{22}\text{Na}$ reaction. It can also be seen from the visual that the difference between the results produced by the DOMP2, DOMP3, DOMP 4 and DOMP 5 models becomes relatively more visible with the increase in the incoming particle energy. Although it is seen that all models exhibit a distribution similar to that of the experimental data in general, it is understood from both Figure 2 and the numerical values available in Table 1 that DOMP1 produces more consistent results compared to other models when the whole energy range is considered.

In this study, the first reaction in which the effects of using different alpha optical model potentials on the calculations were examined is the $^{\text{nat}}\text{Mg}(\alpha,\text{x})^{22}\text{Na}$ reaction. The results of the calculations obtained by triggering a total of eight different models separately are visualized in Figure 3 together. Figure 3 also shows the experimental data of this reaction that Lange et al. [64] brought to the literature with their work. It can be easily seen from Figure 3 that the model developed according to Table 1 in Demetriou et al.'s [56] study, represented by AOMP3 in this work, among the eight models employed in the calculations, provides cross-section results at

lower values than the other models in the entire examined experimental energy range. In addition, it can be said that AOMP7 around the top of the first hump and AOMP2 after the incoming particle energy region of about 75 MeV produce higher cross-section values compared to other models. Models that can be said to produce results with very close values are also noticeable in Figure 3. Since it would be more appropriate to use numerical analysis instead of visual analysis in such cases, the results of the calculations made for this purpose are presented in Table 2. As it can be understood from the presented values, the model that produces more consistent results with the experimental data for the $^{\text{nat}}\text{Mg}(\alpha,x)^{22}\text{Na}$ reaction is AOMP6 according to the F parameter, while it is AOMP5 according to the D parameter. It will be necessary to emphasize that F also takes into account the error in the experimental data, while D does not, recalling the section of this work where the difference between the F and D parameters is described.

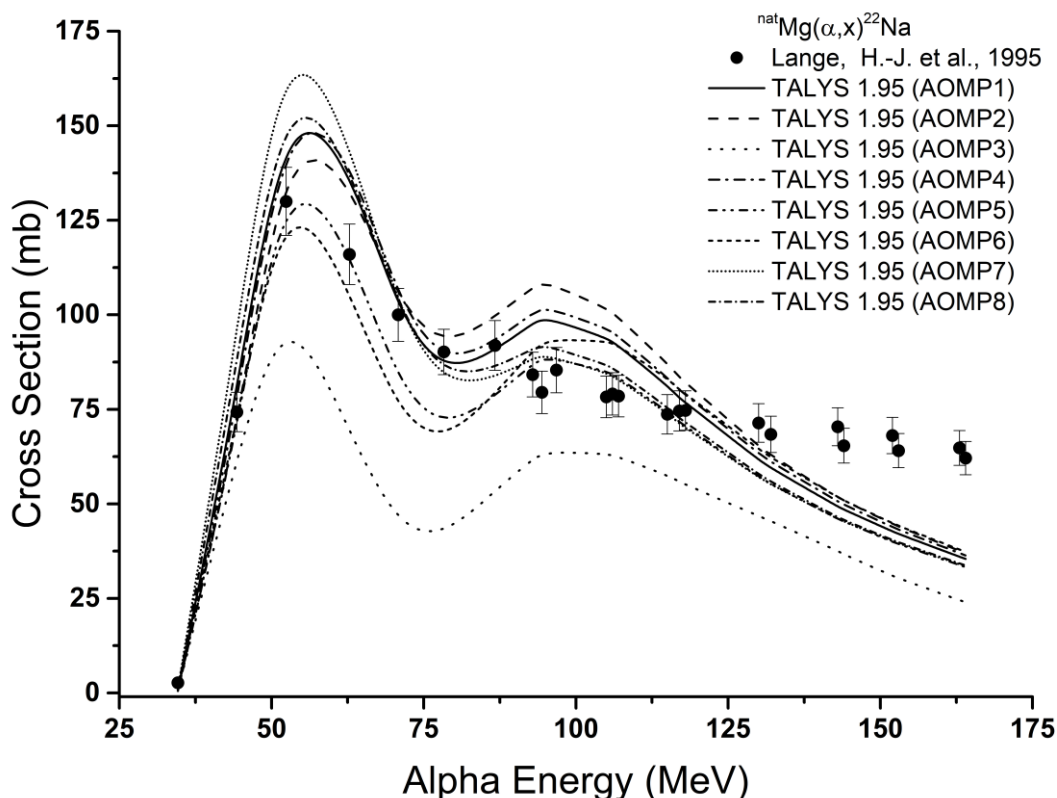


Figure 3. Calculation results and experimental data for the $^{\text{nat}}\text{Mg}(\alpha,x)^{22}\text{Na}$ reaction

The results of the $^{\text{nat}}\text{Mg}(\alpha,x)^{24}\text{Na}$ reaction, the last reaction examined within the scope of the study, are depicted together with the experimental data of Nozaki et al. [65] and Lange et al. [64] in Figure 4. In this reaction, the experimental data of Nozaki et al. [65] were limited in the region shown with the incoming particle energy range of 35-50 MeV in Figure 4, while the experimental data of Lange et al. [64] showed a distribution in a wider energy area and higher energy value. As a result of the evaluation of the experimental data as a whole, it can be easily said from Figure 4 that while the calculation results showed a relatively consistent but quite similar hump structure among themselves, this was not valid after approximately 65 MeV of the experimental data. It can be seen that in the top region of the hump structure AOMP2 produced higher cross-section values than the others from all the utilized models. On the other

hand, the model that produced the lowest cross-section value in the same area was AOMP3. The numerical results of the F and D values given in Table 2 are higher than the results obtained for $^{\text{nat}}\text{Mg}(\alpha,x)^{22}\text{Na}$ due to the fact that the calculation results are not in clear agreement with the experimental data in general. As a result of the comparisons made according to the energy range of the experimental data, the model, which managed to produce more compatible results with the experimental data in the whole energy range according to the F and D values compared to the other options, is highlighted as AOMP6 as can be seen from the numerical values available in Table 2.

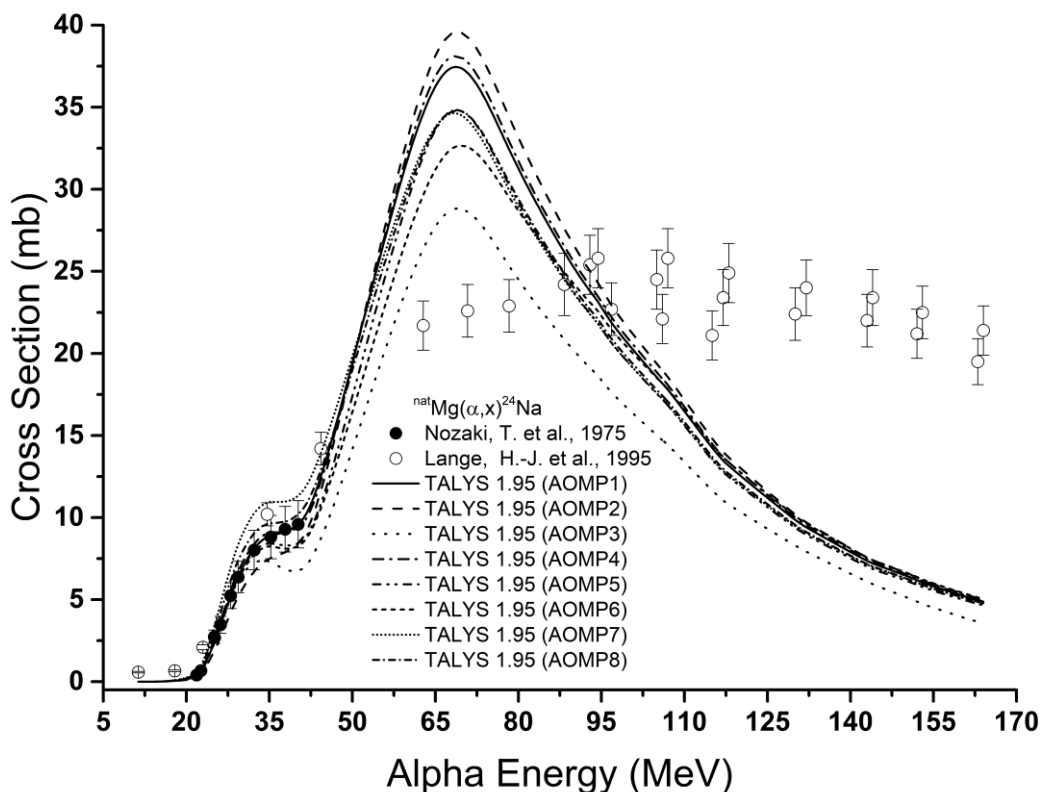


Figure 4. Calculation results and experimental data for the $^{\text{nat}}\text{Mg}(\alpha,x)^{24}\text{Na}$ reaction

4. Conclusion

This section presents a holistic evaluation of all outputs by evaluating all findings obtained in accordance with the steps taken while adhering to the motivation of this study, which is explained in the preceding sections. The first remarkable result is the differences in cross-section calculation values depending on the incoming particle type and energy, which has been observed by considering all the reactions studied. Although the incoming particle energies in the deuteron induced $^{\text{nat}}\text{Mg}(\text{d},x)^{22}\text{Na}$ and $^{\text{nat}}\text{Mg}(\text{d},x)^{24}\text{Na}$ reactions are in the range of 0-50 MeV, as can be seen from the figures, it is clearly seen that the limits of the cross-section values obtained and shown on the y-axis are different. This situation is also clearly seen in the alpha induced $^{\text{nat}}\text{Mg}(\alpha,x)^{22}\text{Na}$ and $^{\text{nat}}\text{Mg}(\alpha,x)^{24}\text{Na}$ reactions with incoming particle energies of 25-175 MeV and 0-170 MeV, respectively. Of course, the fact that the reaction processes are different by their nature is a factor in the formation of this situation, and there are different physical processes that has been experienced during the formation of the reaction routes investigated.

Another important point to be mentioned is how the use of models and parameters in theoretical calculations in which they are employed affects the results. It is clear from both the graphs and the numerical calculations performed with the calculation results obtained that the differentiation of the model or parameters used even in the same reaction can cause easily understandable differences in the results. The use of different models in the reactions examined in this study, in which deuteron and alpha optical model potentials were utilized, directly affected the cross-section results.

Among the reactions examined in this study, it can be easily seen from the figures and tables that the calculation results of both the deuteron induced $^{\text{nat}}\text{Mg}(\text{d},\text{x})^{22}\text{Na}$ and $^{\text{nat}}\text{Mg}(\text{d},\text{x})^{24}\text{Na}$ reactions exhibit harmony with the experimental data. For both reactions, both F and D values highlights the model abbreviated as DOMP1, which is the one used as the default model by TALYS, as the model that produces the most compatible results with the experimental data. In the alpha induced reactions, a harmony was observed between the experimental data and the calculation results for the $^{\text{nat}}\text{Mg}(\alpha,\text{x})^{22}\text{Na}$ reaction, while a similar agreement could not be seen in the entire energy range for the $^{\text{nat}}\text{Mg}(\alpha,\text{x})^{24}\text{Na}$ reaction, unfortunately. The F value, which includes the margins of error in the experimental data, revealed the AOMP6 model as the model that produced more compatible results with the experimental data in both $^{\text{nat}}\text{Mg}(\alpha,\text{x})^{22}\text{Na}$ and $^{\text{nat}}\text{Mg}(\alpha,\text{x})^{24}\text{Na}$ reactions. On the other hand, according to D values, AOMP5 was pointed in the $^{\text{nat}}\text{Mg}(\alpha,\text{x})^{22}\text{Na}$ reaction, while AOMP6 was highlighted in the $^{\text{nat}}\text{Mg}(\alpha,\text{x})^{24}\text{Na}$ reaction. Here, it will be useful to consider the differences between the numerical data, as well as the differences in the calculation methods of the F and D values, as explained earlier.

In the absence of experimental data, it is very important to choose the model or parameter that will provide more compatible results with the experimental data in the theoretical calculations that lead to very useful results for researchers. For this reason, with this and similar studies, a more detailed analysis of models and parameters can be made and various improvements can be achieved. From this point of view, it is necessary to contribute to the literature by conducting similar studies for different reactions too.

Ethics in Publishing

There are no ethical issues regarding the publication of this study.

Author Contributions

Mert Şekerci: Designing the study, performing the calculations, evaluating the results, writing the article.

References

[1] Özdoğan, H., Şekerci, M., Kaplan, A. (2020). An investigation on the effects of some theoretical models in the cross-section calculations of $^{50,52,53,54}\text{Cr}(\alpha,\text{x})$ reactions. *Physics of Atomic Nuclei*, 83, 820–827.

- [2] Yiğit, M., Tel, E. (2014). Theoretical study of deuteron induced reactions on $^{6,7}\text{Li}$, ^9Be and ^{19}F targets. *Kerntechnik*, 79, 63-69.
- [3] Kavun, Y., Aydın, A., Tel, E. (2020). A new formulae study for the (n,2p) reaction cross-section systematics at 14–15 MeV. *Applied Radiation and Isotopes*, 163, 109218.
- [4] Tel, E., Akca, S., Kara, A., Yiğit M., Aydın A. (2013). (p, α) reaction cross sections calculations of Fe and Ni target nuclei using new developed semi-empirical formula. *Journal of Fusion Energy*, 32, 531–535.
- [5] Artun, O. (2018). Calculation of productions of PET radioisotopes via phenomenological level density models. *Radiation Physics and Chemistry*, 149, 73-83.
- [6] Yiğit, M., Bostan, S. N. (2019). Study on cross section calculations for (n,p) nuclear reactions of cadmium isotopes. *Applied Radiation and Isotopes*, 154, 108868.
- [7] Artun, O. (2019). Calculation of productions of medical ^{201}Pb , ^{198}Au , ^{186}Re , ^{111}Ag , ^{103}Pd , ^{90}Y , ^{89}Sr , ^{77}Kr , ^{77}As , ^{67}Cu , ^{64}Cu , ^{47}Sc and ^{32}P nuclei used in cancer therapy via phenomenological and microscopic level density models. *Applied Radiation and Isotopes*, 144, 64-79.
- [8] Akkoyun, S. (2020). Estimation of fusion reaction cross-sections by artificial neural networks. *Nuclear Instruments and Methods in Physics Research Section B*, 462, 51-54.
- [9] Özdoğan, H., Üncü, Y. A., Şekerci, M., Kaplan, A. (2021). Estimations of level density parameters by using artificial neural network for phenomenological level density models. *Applied Radiation and Isotopes*, 169, 109583.
- [10] Özdoğan, H., Üncü, Y. A., Şekerci, M., Kaplan, A. (2021). A study on the estimations of (n, t) reaction cross-sections at 14.5 MeV by using artificial neural network. *Modern Physics Letters A*, 36(23), 2150168.
- [11] Özdoğan, H., Üncü, Y. A., Karaman, O., Şekerci, M., Kaplan, A. (2021). Estimations of giant dipole resonance parameters using artificial neural network. *Applied Radiation and Isotopes*, 169, 109581.
- [12] Şekerci, M., Özdoğan, H., Kaplan, A. (2022). Effects of combining some theoretical models in the cross-section calculations of some alpha-induced reactions for natSb. *Applied Radiation and Isotopes*, 186, 110255.
- [13] Özdoğan, H., Üncü, Y. A., Şekerci, M., Kaplan, A. (2022). Mass excess estimations using artificial neural networks. *Applied Radiation and Isotopes*, 184, 110162.
- [14] Aydın, A., Tel, E., Kaplan, A., Büyüksulu, H. (2010). Pre-equilibrium cross section calculations in alpha induced reactions on ^{65}Cu and ^{209}Bi , *Annals of Nuclear Energy*, 37(10), 1316-1320.

- [15] Kaplan, A., Büyüksulu, H., Aydın, A., Tel, E., Yıldırım, G., Bölükdemir, M. H. (2010). Excitation Functions of Some Neutron Production Targets on (d,2n) Reactions, *Journal of Fusion Energy*, 29, 181-187.
- [16] Büyüksulu, H., Kaplan, A., Tel, E., Aydın, A., Yıldırım, G. (2010). Neutron Emission Spectra of $^{104,105,106,108,110}\text{Pd}$ Isotopes for (p,xn) Reactions at 21.6 MeV Proton Incident Energy, *Journal of Fusion Energy*, 29, 41-48.
- [17] Broeders, C. H. M., Konobeyev, A. Yu., Korovin, Yu. A., Lunev, V. P., Blann, M. (2006). "ALICEIASH - Pre-compound and evaporation model code system for calculation of excitation functions, energy and angular distributions of emitted particles in nuclear reactions at intermediate energies". FZK 7183.
- [18] Gudima, K. K., Mashnik, S. G., Toneev, V. D. (1983). Cascade-exciton model of nuclear reactions, *Nuclear Physics A*, 401(2), 329–361.
- [19] Mashnik, S. G. (1995). User Manual for the Code CEM95, Joint Institute for Nuclear Research, Dubna, Moscow.
- [20] Capote, R., Lopez, R., Herrera, E., Piris, M., Osorio, V. (1991). Analysis of experimental data on neutron induced reactions and development of PCROSS code for the calculation of the differential preequilibrium spectra, INDC(NDS)-247/L, International Atomic Energy Agency (IAEA), Vienne.
- [21] Herman, M., Capote, R., Carlson, B. V., Obložinský, P., Sin, M., Trkov, A., Wienke, H., Zerkin, V. (2007). EMPIRE: Nuclear Reaction Model Code System for Data Evaluation. *Nuclear Data Sheets*, 108(12), 2655-2715.
- [22] Koning A. J., Hilaire, S., Duijvestijn, M. C. (2008). TALYS-1.0, Proceedings of the International Conference on Nuclear Data for Science and Technology, April 22-27, 2007, Nice, France, editors Bersillon, O., Günsing, F., Bauge, E., Jacqmin, R., Leray, S., EDP Sciences, 2008, p. 211-214.
- [23] Koning, A., Hilaire, S., Goriely, S. (2019). TALYS–1.95 A Nuclear Reaction Program, User Manual, first ed. NRG, The Netherlands.
- [24] Tel, E., Aydın, E. G., Kaplan, A., Aydın, A. (2009). New Calculations of Cyclotron Production Cross Sections of Some Positron Emitting Radioisotopes in Proton Induced Reactions. *Indian Journal of Physics*, 83(2), 193-212.
- [25] Aydın, A., Tel, E., Pekdoğan, H., Kaplan, A. (2012). Nuclear Model Calculations on the Production of $^{125,123}\text{Xe}$ and $^{133,131,129,128}\text{Ba}$ Radioisotopes. *Physics of Atomic Nuclei*, 75(3), 310-314.
- [26] Tel, E., Aydın, A., Kara, A., Kaplan, A. (2012). Investigation of Ground State Features for Some Medical Radionuclides Using an effective Nuclear Force. *Kerntechnik*, 77 (1), 50-55.

- [27] Canbula, B. (2017). Bazı tellür izotoplarının nötron yakalama tesir kesiti analizi, *Celal Bayar Üniversitesi Fen Bilimleri Dergisi*, 13(2), 445-455.
- [28] Kurenkov, N. V., Lunev, V. P., Shubin, Yu. N. (1999). Evaluation of calculation methods for excitation functions for production of radioisotopes of iodine, thallium and other elements, *Applied Radiation and Isotopes*, 50(3), 541-549.
- [29] Audi, G., Bersillon, O., Blachot, J., Wapstra, A. H. (2003). The Nubase evaluation of nuclear and decay properties, *Nuclear Physics A*, 729(1), 3–128.
- [30] Haynes, W. M., Lide, D.R., Bruno, T. J. (2017). CRC Handbook of Chemistry and Physics, 97th ed., CRC Press: Boca Raton, FL.
- [31] Greenwood, N. N., Earnshaw, A. (1997). Chemistry of the Elements, 2nd Edition, Butterworth-Heinemann.
- [32] Kondev, F. G., Wang, M., Huang, W. J., Naimi, S., Audi, G. (2021). The NUBASE2020 evaluation of nuclear physics properties, *Chinese Physics C*, 45(3), 030001.
- [33] Al Faraj, A., Alotaibi, B., Pasha Shaik, A., Shamma, K., Al Jammaz, I., Gerl, J. (2015). Sodium-22-radiolabeled silica nanoparticles as new radiotracer for biomedical applications: in vivo positron emission tomography imaging, biodistribution, and biocompatibility. *International Journal of Nanomedicine*, 6293-6302.
- [34] Akamatsu, G., Yoshida, E., Mikamoto, T., Maeda, T., Wakizaka, H., Tashima, H., Wakitani, Y., Matsumoto, M., Yamaya, T. (2019). Development of sealed ^{22}Na phantoms for PET system QA/QC: uniformity and stability evaluation. 2019 IEEE Nuclear Science Symposium and Medical Imaging Conference (NSS/MIC).
- [35] Murata, T., Miwa, K., Miyaji, N., Wagatsuma, K., Hasegawa, T., Oda, K., Umeda, T., Iimori, T., Masuda, Y., Terauchi, T., Koizumi, M. (2016). Evaluation of spatial dependence of point spread function-based PET reconstruction using a traceable point-like ^{22}Na source. *EJNMMI Physics*, 3(1), 26.
- [36] Lees, M., Dombrowski, J., Botkin, C., Hubble, W., Nguyen, N., Osman, M. (2008). Utilization of ^{22}Na PET markers in radiation therapy planning: Initial experience. *Journal of Nuclear Medicine*, 49(1), 431.
- [37] Laing, P. G., Ferguson Jr, A. B. (1958). Sodium-24 as an indicator of the blood supply of bone. *Nature*, 182(4647), 1442-1443.
- [38] Scanlon, E. F., Milland, F. P., Hellman, L. (1990). Sodium-24 studies in postmastectomy lymphedema. *Journal of Surgical Oncology*, 44(1), 47-51.
- [39] Kety, S. S. (1948). Quantitative measurement of regional circulation by the clearance of radioactive sodium. *The American Journal of the Medical Sciences*, 215 (3), 352.

- [40] Moulton, R., Spencer, A. G., Willoughby, D. A. (1958). Noradrenaline sensitivity in hypertension measured with a radioactive sodium technique. *British Heart Journal*, 20(2), 224-228.
- [41] Gülümser, T., Kaplan, A. (2021). A theoretical study on the production cross-section calculations for ^{24}Na medical isotope. *Erzincan Üniversitesi Fen Bilimleri Enstitüsü Dergisi*, 14(2), 802-813.
- [42] Guo, S., Zhang, J., Shi, L., Chen, Q., Chen, W. K. (2022). Research on the application of ^{22}Na radiolocation detection technology in advanced manufacturing process control. *Kerntechnik*, 87(3), 316-322.
- [43] Yoshida, A., Kambara, T., Nakao, A., Uemoto, R., Uno, H., Nagano, A., Yamaguchi, H., Nakao, T., Kahl, D., Yanagisawa, Y., Kameda, D., Ohnishi, T., Fukuda, N., Kubo, T. (2013). Wear diagnostics of industrial material using RI beams of ^7Be and ^{22}Na . *Nuclear Instruments and Methods in Physics Research Section B*, 317, 785-788.
- [44] Pant, H. J., Sharma, V. K., Nair, A. G. C., Tomar, B. S., Nathaniel, T. N., Reddy, A. V. R., Singh, G. (2009). Application of ^{140}La and ^{24}Na as intrinsic radiotracers for investigating catalyst dynamics in FCCUs. *Applied Radiation and Isotopes*, 67(9), 1591-1599.
- [45] Epp, E. M., Griffin, H. C. (2003). Use of ^{24}Na as a γ -ray calibration source above 3MeV. *Nuclear Instruments and Methods in Physics Research Section A*, 505(1-2), 9-12.
- [46] Raynal, J. (1994). Notes on ECIS94 CEA Saclay Report No. CEA-N-2772.
- [47] Koning, A. J., Rochman, D. (2012). Modern Nuclear Data Evaluation with the TALYS Code System, *Nuclear Data Sheets*, 113(12), 2841-2934.
- [48] Watanabe, S. (1958). High energy scattering of deuterons by complex nuclei. *Nuclear Physics*, 8, 484-492.
- [49] Daehnick, W. W., Childs, J. D., Vrcelj, Z. (1980). Global optical model potential for elastic deuteron scattering from 12 to 90 MeV. *Physical Review C*, 21, 2253-2274.
- [50] Bojowald, J., Machner, H., Nann, H., Oelert, W., Rogge, M., Turek, P. (1988). Elastic deuteron scattering and optical model parameters at energies up to 100 MeV. *Physical Review C*, 38, 1153-1163.
- [51] Han, Y., Shi, Y., Shen, Q. (2006). Deuteron global optical model potential for energies up to 200 MeV. *Physical Review C*, 74, 044615.
- [52] An, H., Cai, C. (2006). Global deuteron optical model potential for the energy range up to 183 MeV. *Physical Review C*, 73, 054605.
- [53] Avrigeanu, V., Avrigeanu, M., Mănăilescu, C. (2014). Further explorations of the α -particle optical model potential at low energies for the mass range $A \approx 45-209$. *Physical Review C*, 90, 044612.

- [54] Koning, A. J., Delaroche, J. P. (2003). Local and global nucleon optical models from 1 keV to 200 MeV. *Nuclear Physics A*, 713, 231-310.
- [55] McFadden, L., Satchler, G. R. (1966). Optical-model analysis of the scattering of 24.7 MeV alpha particles. *Nuclear Physics*, 84, 177-200
- [56] Demetriou, P., Grama, C., Goriely, S. (2002). Improved global α -optical model potentials at low energies. *Nuclear Physics A*, 707, 253-276.
- [57] Nolte, M., Machner, H., Bojowald, J. (1987). Global optical potential for α particles with energies above 80 MeV. *Physical Review C*, 36, 1312-1316.
- [58] Avrigeanu, V., Hodgson, P. E., Avrigeanu, M. (1994). Global optical potentials for emitted alpha particles. *Physical Review C*, 49, 2136-2141.
- [59] Otuka, N., Dupont, E., Semkova, V., Pritychenko, B., Blokhin, A. I., Aikawa, M., Babykina, S., Bossant, M., Chen, G., Dunaeva, S., Forrest, R. A., Fukahori, T., Furutachi, N., Ganesan, S., Ge, Z., Gritzay, O. O., Herman, M., Hlavač, S., Katō, K., Lalremruata, B., Lee, Y. O., Makinaga, A., Matsumoto, K., Mikhaylyukova, M., Pikulina, G., Pronyaev, V. G., Saxena, A., Schwerer, O., Simakov, S. P., Soppera, N., Suzuki, R., Takács, S., Tao, X., Taova, S., Tárkányi, F., Varlamov, V. V., Wang, J., Yang, S. C., Zerkin, V. (2014). Towards a More Complete and Accurate Experimental Nuclear Reaction Data Library (EXFOR): International Collaboration Between Nuclear Reaction Data Centres (NRDC). *Nuclear Data Sheets*, 120, 272-276.
- [60] Zerkin, V. V., Pritychenko, B. (2018). The experimental nuclear reaction data (EXFOR): Extended computer database and Web retrieval system. *Nuclear Instruments and Methods in Physics Research Section A*, 888, 31-43.
- [61] Hermanne, A., Takács, S., Tárkányi, F., Adam-Rebeles, R., Ignatyuk, A. (2012). Excitation functions for ^7Be , $^{22,24}\text{Na}$ production in Mg and Al by deuteron irradiations up to 50MeV. *Applied Radiation and Isotopes*, 70(12), 2763-2772.
- [62] Vlasov, N. A., Kalinin, S. P., Ogloblin, A. A., Pankratov, V. M., Rudakov, V. P., Serikov, I. N., Sidorov, V. A. (1957). Excitation functions for the reactions $^{24}\text{Mg}(d,\alpha)^{22}\text{Na}$, $^{54}\text{Fe}(d,\alpha)^{52}\text{Mn}$, $^{54}\text{Fe}(d,n)^{55}\text{Co}$, $^{66}\text{Zn}(d,2n)^{66}\text{Ga}$. *Atomnaya Energiya*, 12, 169.
- [63] Wilson, R. L., Frantsvog, D. J., Kunselman, A. R., Détraz, C., Zaidins, C. S. (1976). Excitation functions of reactions induced by 1H and 2H ions on natural Mg, Al, and Si. *Physical Review C*, 13, 976 - 983.
- [64] Lange, H.-J., Hahn, T., Michel, R., Schiekel, T., Rösel, R., Herpers, U., Hofmann, H.-J., Dittrich-Hannen, B., Suter, M., Wölfli, W., Kubik, P. W. (1995). Production of residual nuclei by α -induced reactions on C, N, O, Mg, Al and Si up to 170 MeV. *Applied Radiation and Isotopes*, 46(2), 93-112.
- [65] Nozaki, T., Furukawa, M., Kume, S., Seki, R. (1975). Production of ^{28}Mg by triton and α -particle induced reactions. *Applied Radiation and Isotopes*, 26(1), 17-20.